Neuro-Oncology Advances
6(1), vdae184, 2024 | https://doi.org/10.1093/noajnl/vdae184 | Advance Access date 2 November 2024

Cell migration simulator-based biomarkers for glioblastoma

Jay Hou, Mariah McMahon, Tyler Jubenville, Jann N. Sarkaria, Clark C. Chen, and David J. Odde

All author affiliations are listed at the end of the article

Corresponding Author: David J. Odde, PhD, Department of Biomedical Engineering, University of Minnesota—Twin Cities, 312 Church St. SE, RM7-240 Nils Hasselmo Hall, Minneapolis, MN 55455, USA (oddex002@umn.edu).

Abstract

Background. Glioblastoma is the most aggressive malignant brain tumor with poor survival due to its invasive nature driven by cell migration, with unclear linkage to transcriptomic information. The aim of this study was to develop a physics-based framework connecting to transcriptomics to predict patient-specific glioblastoma cell migration.

Methods and Results. We applied a physics-based motor-clutch model, a cell migration simulator (CMS), to parameterize the migration of glioblastoma cells and define physical biomarkers on a patient-by-patient basis. We reduced the 11-dimensional parameter space of the CMS into 3 principal physical parameters that govern cell migration: motor number—describing myosin II activity, clutch number—describing adhesion level, and F-actin polymerization rate. Experimentally, we found that glioblastoma patient-derived (xenograft) cell lines across mesenchymal (MES), proneural, and classical subtypes and 2 institutions ($N = 13$ patients) had optimal motility and traction force on stiffnesses around 9.3 kPa, with otherwise heterogeneous and uncorrelated motility, traction, and F-actin flow. By contrast, with the CMS parameterization, we found that glioblastoma cells consistently had balanced motor/clutch ratios to enable effective migration and that MES cells had higher actin polymerization rates resulting in higher motility. The CMS also predicted differential sensitivity to cytoskeletal drugs between patients. Finally, we identified 18 genes that correlated with the physical parameters, suggesting transcriptomic data alone could potentially predict the mechanics and speed of glioblastoma cell migration.

Conclusions. We describe a general physics-based framework for parameterizing individual glioblastoma patients and connecting to clinical transcriptomic data that can potentially be used to develop patient-specific anti-migratory therapeutic strategies.

Key Points

- Glioblastoma cells had balanced motor/clutch ratios to enable effective migration.
- Mesenchymal cells had enhanced actin polymerization resulting in higher motility.
- Eighteen genes were correlated with the biophysical parameters to predict cell migration.

Glioblastoma is the most common malignant brain tumor with a median survival of only 15 months and less than 5% 5-year survival rate.[1,2] Complete surgical resection is difficult because the tumor is highly invasive, and tumor cell infiltration into the surrounding brain tissue drives disease progression and recurrence.[3,4] Therefore, understanding the mechanics of cancer cell migration can potentially be used to predict patterns of invasion and guide efforts to disrupt migration and slow disease progression.[5] To target cell migration, cilengitide inhibits adhesion proteins such as αvβ3 and αvβ5 integrin but failed in a phase 3 trial,[6] suggesting that other adhesion proteins, such as CD44, serve as major adhesive molecules in glioblastoma.[7–9] Inhibiting nonmuscle myosin II resulted in blocking glioma cell migration,[10,11] and clinically safe derivatives of a myosin

Importance of the Study

Successful precision medicine requires biomarkers to define patient states and identify personalized treatments. While biomarkers are generally based on expression levels of protein and/or RNA, we ultimately seek to alter fundamental cell behaviors such as cell migration, which drives tumor invasion and metastasis. Our study defines a new approach for using biophysics-based models to define mechanical biomarkers that can be used to identify patient-specific anti-migratory therapeutic strategies.

inhibitor are under development.[12] Fluvoxamine, an antidepressant, can potently inhibit actin polymerization and block glioma cell migration.[13] However, in these studies, the connection of drug potency to fundamental glioma cell migration mechanics as a function of the transcriptomicly defined glioblastoma subtypes of proneural (PN), classical (CL), and mesenchymal (MES)[14–16] was still unclear. In addition, it is not always feasible clinically to conduct in vitro migration assays on patient cells, and different harvesting and culturing methods may significantly alter the migration behavior.[17] Therefore, to effectively target cancer cell migration, it is critical to understand the fundamental mechanics of glioblastoma cell migration and its potential link to transcriptomic information to predict tumor cell invasion based on patient-specific omic analysis.

In the classic cell migration cycle, the first step is the extension of a cell protrusion at the leading edge driven by actin polymerization into self-assembled actin filaments (F-actin). F-actin undergoes retrograde flow driven by myosin II (motor)-mediated contraction, leading to protrusion retraction. At the same time, cell adhesion molecule binding to the extracellular environment and subsequent stretching of the actin-adhesion adaptor proteins constitute a molecular "clutch" that resists myosin forces and biases the protrusion toward net extension. The adhesion proteins can form focal adhesions that allow the cell to transmit traction forces onto compliant substrates. This system is known as the motor-clutch mechanism and is widely used to describe cell migration.[18–20] Stochastic simulations of the motor-clutch model[21] have been developed and successfully predict the cell traction force, cell morphology, and F-actin flow on various substrate conditions.[21–23] Beyond single protrusions, the cell nucleates multiple protrusions via F-actin polymerization, each of which can be modeled as a motor-clutch system, with traction forces balancing across the different protrusions. Stochastic perturbations to the force balance due to adhesion bond rupture enable larger-scale cell movements and can define the front and the rear of the cell.[24,25] By imposing a force balance between the protrusions, Bangasser et al.[26] developed a whole-cell motor-clutch model, which we refer to here as the cell migration simulator (CMS, Figure 1A). The CMS has successfully captured the unique cell migration features on substrates with various stiffnesses,[26] various focal adhesion sizes,[27] different viscoelastic properties,[28] different stiffness gradients,[29] within 1D channels,[30] and in brain tissue ex vivo.[5,7,8,31] Therefore, the CMS provides a consistent mechanical framework that can potentially be used to interpret and synthesize cell migration and force measurements of glioblastoma patient-derived (PD) cells across subtypes to predict cell migration.

In this study, we applied migration assays to glioblastoma PD xenograft (PDX) and PD cells (collectively referred to here as "PD(X)"). We explored the ability of the CMS to serve as a physics-based framework for glioblastoma subtypes and PD(X) systems. We used the CMS parameters representing myosin II motors, adhesion protein "clutches," and F-actin polymerization to predict cell migration generally, and then mechanically parameterized glioblastoma cells obtained from a cohort of 11 glioblastoma patients across all 3 subtypes and 2 different culture procedures. Using single-cell migration and force generation data obtained on compliant 2D surfaces, we found distinct parameter sets for glioblastoma patients across subtypes and culture conditions. In addition, the CMS-predicted differential cell migration sensitivities to cytoskeletal drugs between subtypes. Finally, we established correlative links between the CMS parameter values and patient cell transcriptomes. Our results suggest it is feasible to estimate cell migration speeds using mRNA expression, similar to how migration speed can be estimated via machine learning-based detection of features in clinical MRI images.[31] Overall, we describe a consistent physics-based framework for parameterizing individual glioblastoma patients, connected to clinical transcriptomic data, that can potentially be used to develop subtype and patient-specific anti-migratory therapeutic strategies for glioblastoma.

Materials and Methods

Cell Migration Simulator

The detailed governing equations and algorithms of the CMS were described in Bangasser et al.[26] and in Supplementary Methods. Briefly, the CMS comprises multiple protrusions or modules that were nucleated randomly based on the rate k_{mod}. Protrusions were elongated based on the polymerization rate v_{poly}. Protrusions were capped randomly at the rate k_{cap} eliminating further polymerization and removed if the protrusion length was shorter than the minimum length l_{min}. The cell position was determined by the force balance between protrusion forces for modules and the cell body force. Clutches bound and unbound to F-actin based on the clutch binding rate k_{on} and unbinding rate k_{off} (Table 1).

Monte Carlo simulations were conducted using a direct Gillespie Stochastic Simulation Algorithm, the event was executed based on accumulated event rates, including k_{on}, k_{off}, k_{mod}, and k_{cap}, and the next time step t_{step} was determined based on the total event rates $\sum k_i$. The C++ version of the CMS[27] was used to conduct the simulations on the

Mesabi computer cluster at the Minnesota Supercomputing Institute.

Grouped Clutch

Here we used the grouped-clutch algorithm to significantly enhance the computational efficiency by grouping clutches together to have a smaller number of clutches to represent all clutches, which produced equivalent results but with much faster simulations (Supplementary Figure 2). The detailed governing equations and analysis were described in Supplementary Methods.

Parameter Sensitivity and Clustering

The cell migration predictions, including the maximum random motility coefficient (RMC), the maximum traction force, and the minimum F-actin flow over different stiffnesses were generated by the CMS with the changes of the base parameter values (Table 1), plotted in Supplementary Figure 1. The linear regression between the CMS migration predictions Y and the logarithm of parameter ratios was plotted in Supplementary Figure 1. Parameter sensitivity values were determined by the slope of the linear regression normalized by the base prediction values (Y_0) (slope (linear regression)/Y_0). We applied the agglomerative hierarchical clustering to the CMS parameter sensitivities using the linkage function in MATLAB with an average method to identify the main clusters for the CMS parameter sensitivities (Figure 1B).

Glioblastoma Patient Cell Lines and Cell Culture

Mayo PDX cell lines were developed and maintained by the Sarkaria lab at Mayo Clinic (Rochester, MN).[32] Cell lines were established by implanting patient tumors into mouse flanks, and cells were derived in short-term explant cultures with serum-containing medium. We used MES (Mayo 16, 46, 59), PN (Mayo 64, 80, 85), and CL (Mayo 6, 38, 76, 91, 195) cells. Cells were shipped in fetal bovine serum (FBS) media (Dulbecco's modified Eagle's medium [DMEM] + 10% serum) and grown adherently until confluent, and then frozen in 10% DMSO 90% FBS media. Cells prepared for experiments were thawed into a flask coated with 10% Matrigel (Corning 354263) in Neural Stem Cell (NSC) Media (DMEM/F12 (Gibco 11320033) + 1X B-27 Supplement (Gibco 12587010) + 1X Pen/Strep (Corning 45000-650) + 1ng/mL epidermal growth factor/fibroblast growth factor (Peprotech AF10015/Peprotech AF10018B) (added every 2–3 days)). Cells were allowed to recover for several days prior to imaging.

UCSD PD lines[33] were developed and maintained by Clark Chen's Laboratory at the University of Minnesota (formerly at the University of California San Diego). Cell lines were derived and established from MES and PN glioblastoma patients and cultured as neurospheres.[33] UCSD cells prepared for experiments were propagated in ultra-low adhesion flasks (Corning 3814) with NSC Media and were allowed to recover thawing for several days prior to imaging. For adherent culture conditions, UCSD cells were grown on a Matrigel-coated T-flask in an NSC medium for a minimum of 1 week prior to imaging.

Cell Migration, Traction Force, and F-Actin Flow on PA Gels

Polyacrylamide (PA) gels with different stiffnesses (0.7, 4.6, 9.3, and 19.5 kPa) were synthesized following the previous protocols[26] and described in Supplementary Methods. Before imaging, Mayo cells were plated on laminin with media containing 2% serum to promote adhesion. UCSD cells could not adhere to laminin, collagen, or fibronectin, except for Matrigel with no serum. Time-lapse light microscopic images were taken using established protocols[26] and described in Supplementary Methods. Time-lapse phase-contrast images were taken for 10 h to track cell migration using a Nikon EclipseTE200 microscope with a Plan Fluor 10×/0.30NA objective. Time-lapse phase-contrast images were taken for 3 min to measure F-actin flow. Phase-contrast and epifluorescence images were taken before and after glioblastoma cells detached by treatment with 0.05% trypsin to determine the cell traction.

Cell motility (RMCs), cell area, aspect ratio, actin retrograde flow, and traction strain energy were determined based on established protocols[26] and described in Supplementary Methods. Cell motility, area, and aspect ratio were measured for Mayo MES (Mayo 16(patient number), 46, 59), PN (Mayo 64, 80, 85), and CL(Mayo 6, 38, 76, 91, 195) cells and UCSD MES, PN cells. Actin flow was measured for Mayo MES (Mayo 16, 46, 59), PN (Mayo 64, 80, 85), and CL(Mayo 6, 38, 76, 91, 195) cells and UCSD MES, PN cells. Strain energy was measured for Mayo MES (Mayo 16, 46, 59), PN (Mayo 64, 80, 85), and CL (Mayo 6, 38, 76, 91, 195) cells and UCSD MES, PN cells.

Parameterizing Glioblastoma Cell Lines With (n_m, n_c, v_{poly}) Values

CMS predictions ($v_{F\text{-actin}}$ (min), F_{module} (max), Rmc (max)) were linearly interpolated based on a 3-dimensional parameter space defined by n_m, n_c, and v_{poly}. Cell traction force was estimated using the linear relation between module force and experimental strain energy ($F_{module} = 175 * E_{strain}$) based on the U251 maximum strain energy value and the assumption that U251 cells had 7500 clutches in the model.[26] The unique (n_m, n_c, v_{poly}) values were found for each patient to limit the relative errors between CMS and experimental results to within 10% (eg, ($v_{F\text{-actin}}$ (min, model) – $v_{F\text{-actin}}$ (min, patient))/$v_{F\text{-actin}}$ (min, patient) < 10%).

mRNA Expression Analysis

Detailed mRNA expression analysis was described in Supplementary Methods. In short, we derived RNAseq reads per kilobase million (RPKM) expressions of Mayo PDX cells from Vaubel et al.[32] (19 552 genes, www.cbioportal.org). We filtered out genes with geometric means smaller than 1 and with counts in less than 80% of patients to achieve a normal gene expression distribution compared

Table 1. Parameters for the Cellular Level CMS

Parameter	Symbol	Value	Ref.
Total number of myosin motors	n_m	1000	Adjusted
Total number of clutches	n_c	750	Adjusted
Maximum total actin length	A_{tot}	100 μm	*
Maximum actin polymerization rate	v_{poly}	200 nm/s	Adjusted
Maximum module nucleation rate	k_{mod}	1 s^{-1}	*
Module capping rate	k_{cap}	0.001 s^{-1}	*
Initial module length	l_{in}	5 μm	*
Minimum module length	l_{min}	0.1 μm	*
Cell spring constant	k_{cell}	10 000 pN/nm	*
Number of cell body clutches	$n_{c,cell}$	10	*
Substrate spring constant	k_s	0.3–300 pN/nm	Adjusted
Maximum number of module motors	n_m	1000	*
Myosin motor stall force	F_m	2 pN	*
Unloaded actin flow rate	v_m	120 nm/s	*
Maximum number of module clutches	n_c	750	*
Clutch on-rate	k_{on}	1 s^{-1}	*
Unloaded clutch off-rate	k_{off}	0.1 s^{-1}	*
Clutch spring constant	k_c	0.8 pN/nm	*
Characteristic clutch rupture force	F_b	2 pN	*

*Adebowale et al.[28]

with the original distribution (Supplementary Figure 6A and B, 11 752 genes left). We applied the 2-sample *t*-test to the RNAseq-derived mRNA expression levels of Mayo MES and PN lines and derived 1 177 differential genes with $P < .05$ and FC > 2 in the volcano plot (Supplementary Figure 6C). We applied pathway enrichment analysis to these differential genes based on the KEGG database[34] with the false discovery rate (FDR)-adjusted $P < .05$ and derived 29 enriched pathways (Supplementary Figure 7). We derived the actin-motor gene list (34 genes) based on the "Regulation of actin cytoskeleton" pathway, and the clutch gene list (42 genes) based on the "Focal adhesion" and "ECM-receptor interaction" pathways. We applied linear correlation analysis between the mRNA expression ratios of the actin-motor (Figure 5A and B) and clutch (Figure 5C) genes in the 10 Mayo lines used in the present study and their CMS parameter values (v_{poly}, n_m, n_c) (Figure 5A–C), respectively. We derived RNAseq normalized transcripts per kilobase million (TPM) values by RSEM algorithm from The Cancer Genome Atlas (TCGA) Glioblastoma Project (www.cbioportal.org, 151 patients, 20 531 genes). We applied Cox regression analysis between the mRNA expression ratios of the actin-motor (Supplementary Figure 10A) and clutch (Supplementary Figure 10B) genes in a cohort of 66 Mayo patients and their overall survival, and their hazard ratios with 95% confidence interval were sorted and plotted in Supplementary Figure 10, with the significant hazard ratios in red.

Statistics

* Denotes $P < .05$, ** $P < .01$, and *** $P < .001$ derived from the Kruskal-Wallis test with Dunn–Sidak post hoc analysis.

Code and Data Availability

All codes and data will be made available on reasonable request from the corresponding author.

Results

Three CMS Physical Parameters Dictate Cell Migration and Traction Force

To understand the relationship between the CMS parameters and its predictions, we computed the optimal cell motility (RMC), traction force, and F-actin retrograde flow in the range of substrate stiffnesses across a wide range of parameter values (Supplementary Figure 1). Similar to the analysis in Bangasser et al.,[35] the sensitivities of the fold changes in the CMS predictions to the fold changes in parameter values, referred to as the parameter sensitivities, were plotted in Figure 1B. Results showed that clutch-related parameters (n_c, F_b, k_{on}, k_{off}, k_c, Table 1) increased the cell traction force and reduced the F-actin flow, motor-related parameters (n_m, F_m, v_m, Table 1) increased

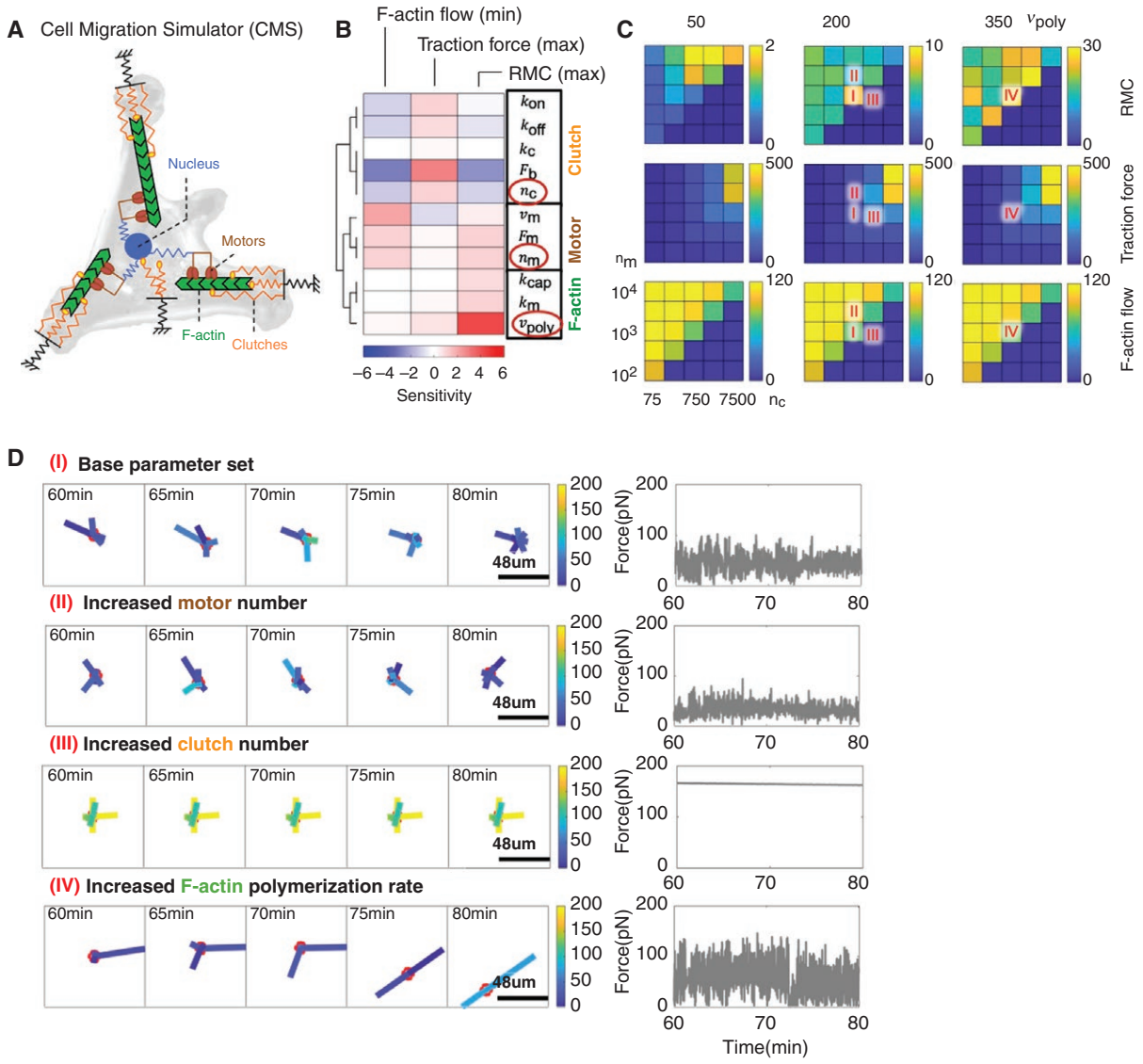

Figure 1. Three cell migration simulator (CMS) physical parameters dictate cell migration and traction force. (A) CMS schematic. (B) Parameter sensitivities of the CMS were analyzed to predict maximum cell migration speed (RMC), minimum F-actin flow, and maximum traction force across substrate stiffnesses. With hierarchical clustering, 3 parameter groups were identified: clutch group (n_c, F_b, k_{on}, k_{off}), motor group (n_m, F_m, v_m) and actin group (v_{poly}, k_{mod}, k_{cap}). The 3 parameters (n_m, n_c, v_{poly}) were chosen as fundamental physical expressions of the CMS. (C) Maximum RMC, maximum traction, and minimum F-actin flow across substrate stiffnesses as a function of the 3 biophysical expressions (n_m, n_c, v_{poly}) predicted by the CMS were plotted. Conditions I–IV represent distinct cell migratory behaviors with different (n_m, n_c, v_{poly}). (D) Condition I represents a typical migrating cell with base parameter values. In Condition II, a higher motor number resulted in lower traction, shorter protrusion length, and slower cell migration. In Condition III, a higher clutch number resulted in near-maximal constant traction, limited dynamic protrusions, and poor cell migration. In Condition IV, a higher actin polymerization rate resulted in more dynamic protrusions, longer protrusion length, highly fluctuating traction, and faster cell migration.

the F-actin flow and motility, and actin-related parameters (k_{mod}, v_{poly}, k_{cap}, Table 1) increased the motility (Figure 1B). We applied unsupervised hierarchical clustering to the parameter sensitivities, and the motor, clutch, and actin-related parameters naturally clustered into motor, clutch, and actin groups, respectively (Figure 1B). Therefore, the CMS parameters can be categorized broadly into 3 groups, and each has its own unique influence on predicted cell migration, which allows us to reduce the 11-dimensional parameter space (see Table 1) to 3 fundamental dimensions of motor, clutch, and actin parameters.

Because of the natural clustering into 3 distinct groups, we chose 1 parameter from each clustered group as the fundamental physical parameters: motor number (n_m) representing myosin II motor activity, clutch number (n_c) representing functional adhesion protein level, and F-actin polymerization rate (v_{poly}) representing actin filament polymerization activity. These 3 parameters are the

key components in the cell migration process,[18–20] they exhibit different values in different cell types,[24,25] and they are easily manipulated by drugs.[26] Therefore, we used these 3 parameters (n_m, n_c, v_{poly}) as a fundamental basis set to predict glioblastoma cell migration across subtypes and culture conditions in the absence and presence of drugs.

To illustrate the cell migration governed by the 3 fundamental physical parameters, we plotted the optimal motility (RMC), traction force, and F-actin flow as a function of the 3 physical parameters (n_m, n_c, v_{poly}) (Figure 1C). Here we used the grouped-clutch algorithm to significantly enhance the computational efficiency (Supplementary Figure2). There are 4 different scenarios observed in the parameter space (Figure 1C, Conditions I–IV), and the time-dependent cell protrusion dynamics and traction force fluctuations in these conditions were plotted in Figure 1D. In Condition I, a typical simulated migrating cell with a balanced motor and clutch number showed the dynamic protrusions with sequential phases of nucleation, elongation, retraction, and elimination, and fluctuating traction force to produce fast cell migration (Figure 1C and D, Condition I). In Condition II with the higher motor number in the cells, the motor-clutch mechanism became "free-flowing"[35] with faster F-actin flow, lower traction force, shorter protrusion length, and hence slower cell migration (Figure 1C and D, Condition II). In Condition III with the higher clutch number, the motor-clutch system became "stalled"[35] with near zero F-actin flow, near-maximal constant traction force, limited dynamic protrusions, and hence poor cell migration (Figure 1C and D, Condition III). In Condition IV with the higher actin polymerization rate, the protrusion dynamics became more significant, with longer protrusion length and highly fluctuating traction forces, to produce faster cell migration (Figure 1C and D, Condition IV). Overall, these simulations indicate that the CMS fundamental parameters (n_m, n_c, v_{poly}) can uniquely describe motor-clutch-mediated cell migration.

Heterogeneity in Migration Phenotypes of Glioblastoma Patient Cells

To understand the migration phenotypes of glioblastoma patient cells, we measured the cell migration of Mayo glioblastoma PDX lines of MES (MM, 3 lines), PN (MP, 3 lines), CL (MC, 5 lines) subtypes with adherent culture[32] and UCSD glioblastoma PD lines of MES (UM, 1 line), PN (UP, 1 line) subtypes cultured as neurospheres[33] ($N = 13$, Figure 2C). We measured the migration of glioblastoma cells on PA gels with different stiffnesses, coated with laminin for the Mayo cells and Matrigel for the UCSD cells, to reach adequate cell adhesion (Figure 2A and B). We found heterogeneity in cell migration of glioblastoma cells with different subtypes and sources, and their mean ± SEM of cell motility (RMC), traction strain energy, and F-actin retrograde flow rate were all highly variable (Figure 2D). Despite this heterogeneity, we found that glioblastoma cells tended to have maximal motility on stiffnesses ranging from 4.6 to 19.5 kPa (Figure 2D), which is comparable to brain tissue stiffnesses (1–6 kPa[36]). Mayo MES and PN cells exhibited optimal traction strain energy with the stiffness of 9.3 kPa, whereas the other cell lines had low cell traction strain energy with no evidence of optimality (Figure 2D). All cell lines had no clear optimal F-actin retrograde flow (Figure 2D), cell area, and aspect ratio (Supplementary Figure 3B) as a function of substrate stiffness. The differences in cell migration between subtypes and sources were similar at all substrate stiffnesses (ie Mayo MES had higher motility than Mayo PN cells at all stiffnesses) (Figure 2D), and therefore, in subsequent analysis, we combined the cell migration data for a given PD(X) line across all substrate stiffnesses.

The mean cell motility (RMC), traction strain energy, and F-actin flow rate for each PD(X) line were plotted in the 3D experimental measurement space with 2D projections (Figure 2E). The cell migration data of all glioblastoma cells across all subtypes and sources were plotted in Supplementary Figure 3C with statistical analysis. Mayo MES cells had significantly higher motility, F-actin flow, cell area, and aspect ratio compared with Mayo PN cells (Figures 2E and Supplementary Figure 3C). Mayo CL cells had intermediate values in motility, F-actin flow, and morphology, except for the lower traction strain energy, compared with Mayo MES, PN cells (Figures 2E and Supplementary Figure 3C). UCSD MES cells had higher motility and cell area compared with UCSD PN cells (Figures 2E and S3C). All Mayo cells had higher traction strain energy, F-actin flow, and cell area with lower motility and aspect ratio compared with all UCSD cells (Figures 2E, and Supplementary Figure 3C). Overall, these results show significant heterogeneity in cell migration mechanics of glioblastoma cells across different subtypes and sources, and a general lack of correlation between motility, traction force, and F-actin flow rate.

CMS-derived parameters of glioblastoma patient cells exhibit balanced motors and clutches with F-actin assembly correlating with cell migration motility.

To transform these empirical measurements of glioblastoma patient cell migration mechanics into fundamental mechanistic interpretation, we used the CMS to parameterize the cell migration of PD(X) lines by fitting their motility, traction force, and F-actin retrograde flow experimental data to simulations with adjusted physical parameters (n_m, n_c, v_{poly}). For each PD(X) line, this effectively mapped the 3D empirical observation space into a 3D theoretical physical space. These physical parameter values were then plotted in the 3D CMS parameter space of (n_m, n_c, v_{poly}) for each patient with 2D projections in Figure 3A, also plotted as bar graphs in Supplementary Figure 4. We found that despite the apparent heterogeneity of physical parameters, glioblastoma PD(X) lines consistently showed approximately balanced motor number and clutch number ($n_c/n_m \sim 0.75$) (Figure 3A), which enabled robust cell migration and traction forces that increased with the motor-clutch level (Figure 1C). Therefore, we can also plot the CMS parameter values on the heat map of various values for (n_m,v_{poly}) with a constant ratio $n_c/n_m = 0.75$ in Figure 3B. We found that Mayo MES cells had higher motor (n_m) and clutch (n_c) numbers, and higher F-actin polymerization rate (v_{poly}) compared with PN cells (Figures 3A and B, and Supplementary Figure 4), resulting in higher motility and F-actin flow. UCSD MES cells had a higher F-actin polymerization rate (v_{poly}) compared with UCSD PN cells, resulting in higher motility. Mayo cells had higher motor and clutch numbers and lower F-actin polymerization to produce higher traction force and lower motility compared with UCSD cells (Figure 3A and B). These results suggested that

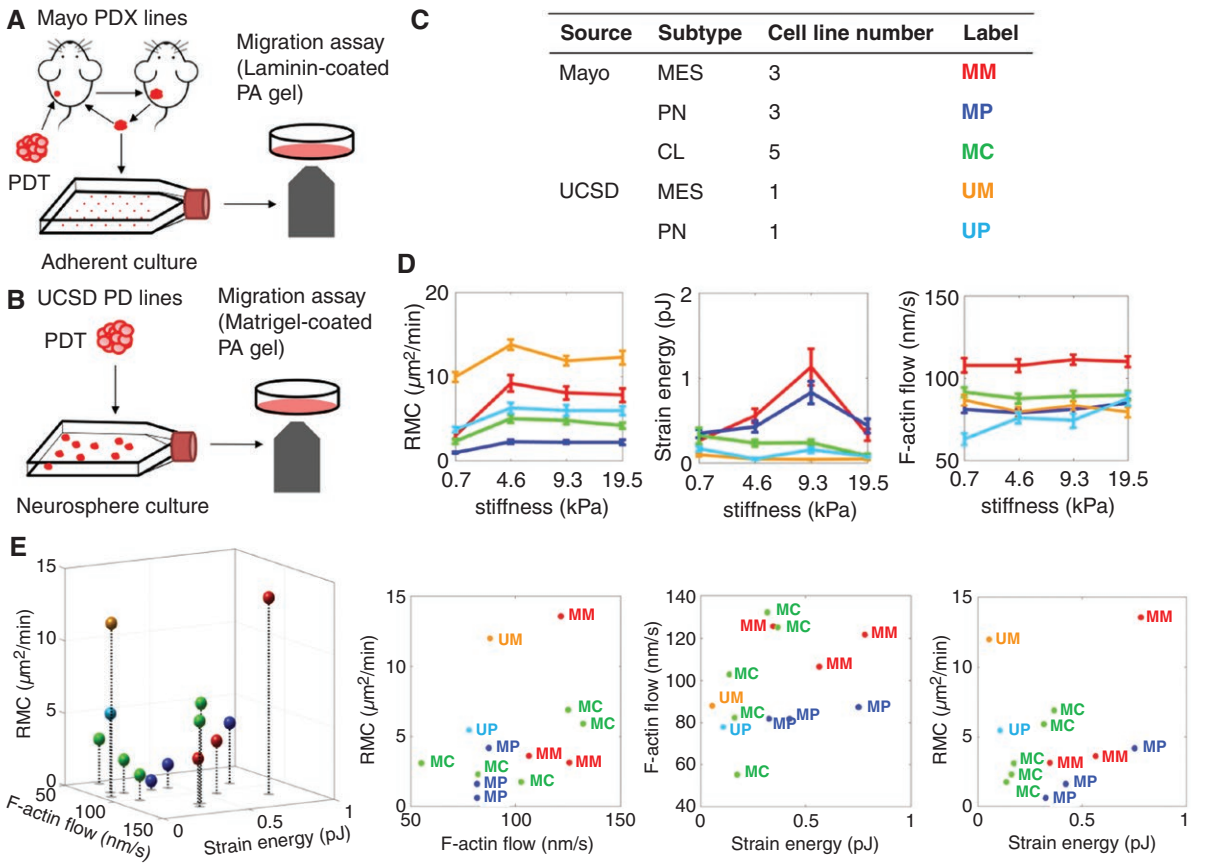

Figure 2. Heterogeneity in migration phenotypes of glioblastoma patient cells. (A) Mayo patient-derived xenograft (PDX) cell lines were established as previously described by implanting patient tumors into mouse flanks[32] and then cultured in adherent conditions with FBS media. (B) UCSD patient-derived (PD) cell lines were established as described previously[33] and cultured in neurosphere conditions with NSC Media. Mayo and UCSD cells were plated on polyacrylamide gels with Young's modulus of 0.7, 4.6, 9.3, and 19.5 kPa, coated with laminin and Matrigel, respectively. Cell motility (random motility coefficient, RMC), traction strain energy, and F-actin retrograde flow were measured using established protocols.[26] (C) There were 3 Mayo MES lines (MM), 3 Mayo PN lines (MP), 5 Mayo CL lines (MC), 1 UCSD MES line (UM), and 1 UCSD PN line (UP). (D) The mean ± SEM values of RMC, strain energy, F-actin flow of Mayo MES, PN, CL cells, and UCSD MES, PN cells on PA gels with different stiffnesses were highly variable across cell lines. (E) The mean values of RMC, strain energy, and F-actin flow combining all substrate stiffnesses for each cell line were plotted in the 3D space, along with their 2D projections. RMC, tractions strain energy, and F-actin flow were all highly variable with no obvious correlations with each other.

myosin motors and adhesion clutches were well balanced in all glioblastoma cells, fast-moving cells had higher F-actin polymerization with either high or low cell traction, and adherently cultured cells had higher myosin motors and adhesion clutches and lower F-actin polymerization compared with neurosphere cultured cells. Overall, the 3D CMS parameter space (n_m, n_c,v_{poly}) provides a more fundamental and revealing framework for describing glioblastoma PD(X) migration than does the empirical 3D space defined by the measured experimental quantities (cell motility (RMC), traction strain energy, F-actin retrograde flow).

The CMS Predicts PD(X) Glioblastoma Cell Migration Upon Drug Perturbations

Knowing the CMS 3D parameter set for each PD(X) line not only allows us to predict the cell migration using the CMS, but also to predict different migration behaviors with the change of parameter values due to hypothetical drug treatments. The CMS predictions with various values of (n_m,v_{poly}) and a constant clutch number ($n_c = 225$) were plotted as the heat map in Figure 4A, along with the UCSD MES cells, which had higher F-actin polymerization rate (v_{poly}) and lower motor number (n_m) (Figure 4A orange) but higher motor/clutch ratio (Figure 3A), resulting in higher cell motility and higher F-actin flow (Figure 4A and B, orange) compared with UCSD PN cells (Figure 4A and B, blue).

When reducing the motor number, the motility and F-actin flow of UCSD MES cells would be reduced to a greater extent than UCSD PN cells as indicated by the solid-red arrows in Figure 4A, which was confirmed by the CMS predictions with the reducing motor number (Δn_m) in Figure 4B. Consistent with the CMS predictions, when UCSD cells were treated with blebbistatin to inhibit their myosin II contractility, the cell motility and F-actin flow of UCSD MES cells on

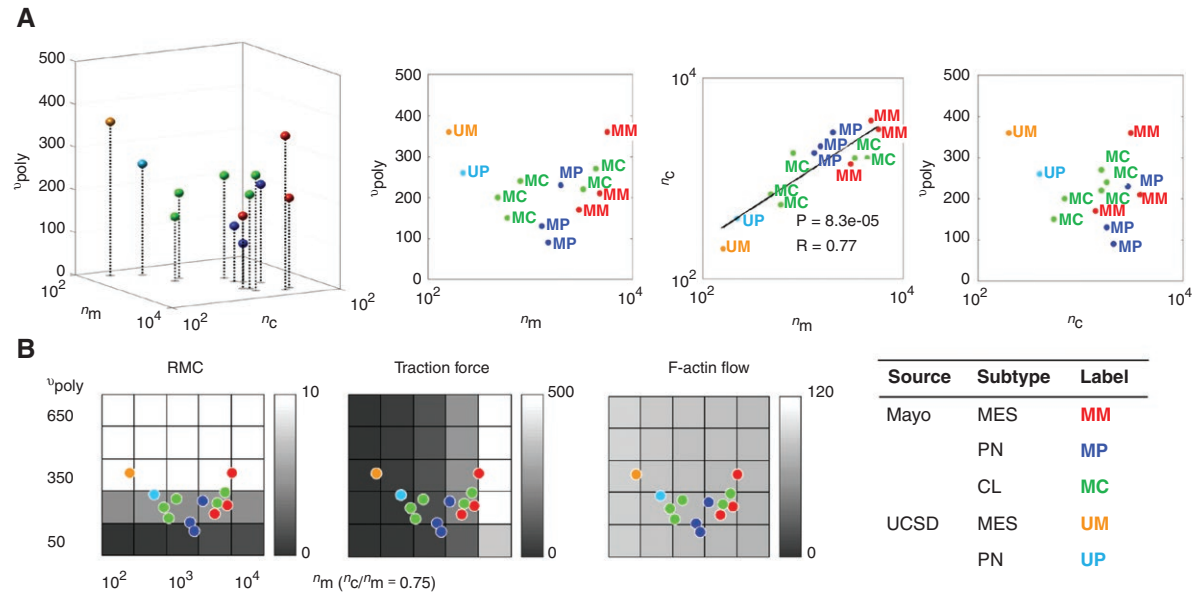

Figure 3. Cell migration simulator (CMS)-derived physical parameters of glioblastoma patient cell migration. (A) Physical parameter values of glioblastoma cells derived by fitting the cell migration with the CMS predictions and plotted in the 3D CMS parameter space of (n_m, n_c, v_{poly}) with 2D projections. (B) Physical parameter values of glioblastoma cells were plotted in the heat map of the CMS prediction with various values for (n_m, v_{poly}) with a constant ratio between n_m and n_c ($n_c/n_m = 0.75$). Given the balanced motor-clutch ratio, cell speed is largely determined by v_{poly}.

PA gels decreased more significantly compared with UCSD PN cells (Figure 4D). This test of the model was not only consistent with the CMS predictions (Figure 4B), but also confirmed the motor number difference between UCSD MES and PN cells (Figures 3A and 4A).

When reducing the F-actin polymerization rate, we predicted that the UCSD PN cells would reduce their motility to a greater extent than UCSD MES cells, with the insensitivity of F-actin flow, as indicated by the dotted arrow in Figure 4A, also confirmed by the CMS predictions with the reducing F-actin polymerization rate, Δv_{poly}, in Figure 4C. We then treated the UCSD cells with Latrunculin A to inhibit their actin polymerization by binding G-actin monomers and found the motility of UCSD PN cells indeed decreased more significantly compared with UCSD MES cells (Figure 4E), which again was consistent with the CMS predictions (Figure 4C).

To test whether the culture conditions affect the migration phenotype, we cultured the neurosphere UCSD MES cells adherently for 1 week to create UCSD MES-AD cells before conducting migration assays, and we found the migration phenotypes of UCSD MES-AD cells became closer to the phenotypes of UCSD PN cells, with higher motor number and lower F-actin polymerization rate resulting in lower motility and higher F-actin flow compared with UCSD MES cells (Supplementary Figure 5A and B). We also treated the UCSD MES-AD cells with cytoskeleton drugs and found MES-AD cells had lower sensitivity to blebbistatin and higher sensitivity to Latrunculin A in motility and F-actin flow compared with UCSD MES cells (Supplementary Figure 5D and E), which again was consistent with the CMS predictions (Supplementary Figure 5B and C), and confirmed that adherent culture can increase the functional motor number and decrease the F-actin polymerization rate of neurosphere cultured cells (Figure S5A).

Overall, we found that CMS-predicted sensitivities of cell motility (Figure 4F) and F-actin flow (Figure 4G) to decreasing parameter values were highly correlated with the measured sensitivities to cytoskeletal drugs. Not only can we use the CMS physical parameter values of glioblastoma PD(X) lines to describe migration phenotypes (Figure 3), but also to predict the differential migration changes between patients due to the changes in the parameter values either by cytoskeletal drugs or by the culture conditions (Figures 4 and Supplementary Figure 5).

Identification of CMS-Based Transcriptomic Biomarkers

In principle, the CMS parameters should depend on transcriptional levels of key genes controlling motor, clutch, and F-actin polymerization activities. Thus, we sought to identify correlates of the CMS parameters in previously collected transcription-level data. In Figures 3 and Supplementary Figure 4, there are consistent differential estimates of the CMS parameters between MES and PN for both Mayo and UCSD patient cells. Moreover, PN and MES subtypes became more frequent in patients with tumor recurrences.[15] Therefore, we decided to analyze the differential genes between MES and PN and correlate them with the CMS parameters. We first derived RNAseq RPKM expression of Mayo PDX cells from Vaubel et al.[32] (19 552 genes in 20 MES patients and 16 PN patients). We filtered out genes with small mean values and low patient

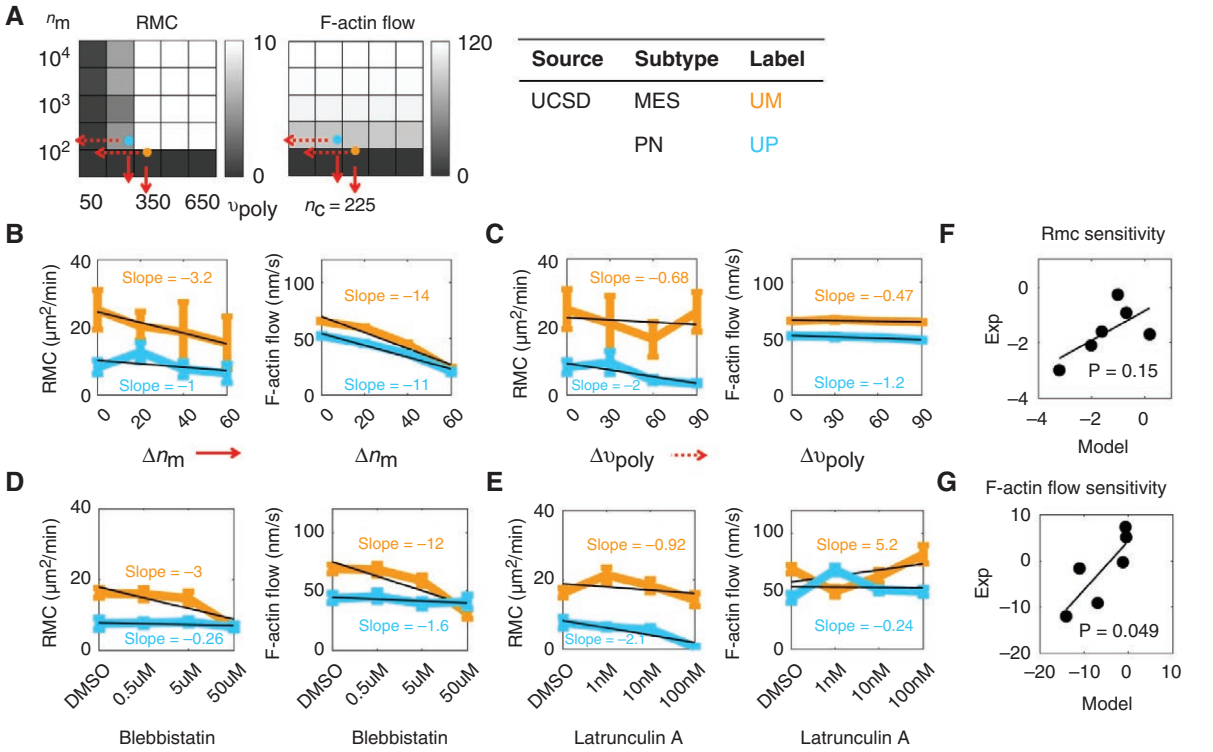

Figure 4. The cell migration simulator (CMS) predicts differential cell migration and F-actin flow sensitivity upon actomyosin drug perturbation. (A) The heat map of the CMS prediction, including motility (RMC) and F-actin retrograde flow, with various values of (n_m, v_{poly}) with a constant value of $n_c = 225$. UCSD MES cells (UM) had a higher F-actin polymerization rate and lower motor number compared with UCSD PN cells (UP), which produced higher motility and higher sensitivity of F-actin flow while reducing the motor number. (B, C) The mean ± SEM values of RMC and F-actin flow of UCSD mesenchymal (MES) and PN cells with the decreasing motor number (B) (solid-red arrow) and decreasing F-actin polymerization rate (C) (dotted-red arrow) predicted by the CMS were plotted. (D, E) The mean ± SEM values of RMC and F-actin flow of UCSD MES and PN cells with different concentrations of myosin II inhibitor, blebbistatin (D), and F-actin polymerization inhibitor, Latrunculin A (E), were plotted. The RMC (F) and F-actin flow (G) sensitivities to decreasing parameter values predicted by the CMS (*x*-axis in (F, G), also slopes in (B, C) and Supplementary Figure 5B and C) were correlated with the sensitivities to cytoskeletal drugs (*y*-axis in (F, G), also slopes in (D, E) and Supplementary Figure 5D and E) with $P = .15$ and $P = .05$, respectively.

portions to achieve a normal gene expression distribution (Supplementary Figure 6A and B, 11 752 genes left). We derived 1177 differential genes between Mayo MES and PN cells using the 2-sample *t*-test ($P < .05$, FC > 2, Supplementary Figure 6C). We applied the pathway enrichment analysis to these differential genes using the KEGG database[34] with the FDR-adjusted $P < .05$ and derived 29 enriched pathways (Supplementary Figure 7). We derived the actin-motor gene list (34 genes) based on the "Regulation of actin cytoskeleton" pathway, and the clutch gene list (42 genes) based on the "Focal adhesion" and "ECM-receptor interaction" pathways. This resulted in a final reduced list of actin-motor and clutch genes that could potentially be correlated with the CMS physical parameters.

We applied correlation analysis between the mRNA expression of the actin-motor and clutch genes in the 10 Mayo PDX lines used in the present study for which mRNA expression level was available, and their CMS parameter values were (v_{poly}, n_m, n_c), respectively. In the correlation of actin-motor genes with the actin polymerization rate, RRAS had the highest positive (although not significant) correlation coefficient (R) and FGFR1 had the lowest (and significant) R (Figure 5A). In the correlation of actin-motor genes with the motor number, VCL, ARPC1B, RRAS2, MSN, ACTN1, ITGB1, RRAS, CXCR4, and MYL12A had statistically significant and positive R ($P < .05$) (Figure 5B). In the correlation of clutch genes with the clutch number, VCL, CD44, EMP1, ACTN1, ITGB1, CAPN2, SHC1, and MYL12A had a positive R that was statistically significant ($P < .05$) (Figure 5C). In Figure 5A and B, altogether, 18 of 76 genes were significantly correlated ($P < 10^{-7}$ for a Poisson distribution with mean = 0.05 × 76 = 4 and observed 18 events) and 17 of 18 genes were positively correlated ($P < 10^{-5}$ for binomial distribution with 17 successes in 18 trials with $P = .05$ success in 1 trial), which is much higher than significance by chance (95% confidence interval, 5% of the 76 total genes = ~4 genes). This result validates the actual correlation of the CMS parameters to the gene expression in cell migration.

With the genes highly correlating with the CMS parameters, we were able to estimate the physical parameters of Mayo PDX lines ($N = 66$) based on their mRNA expressions. RRAS, CXCR4, TMSB4X, RRAS2, and ARPC1B were highly correlated with actin polymerization rate (Figure 5A)

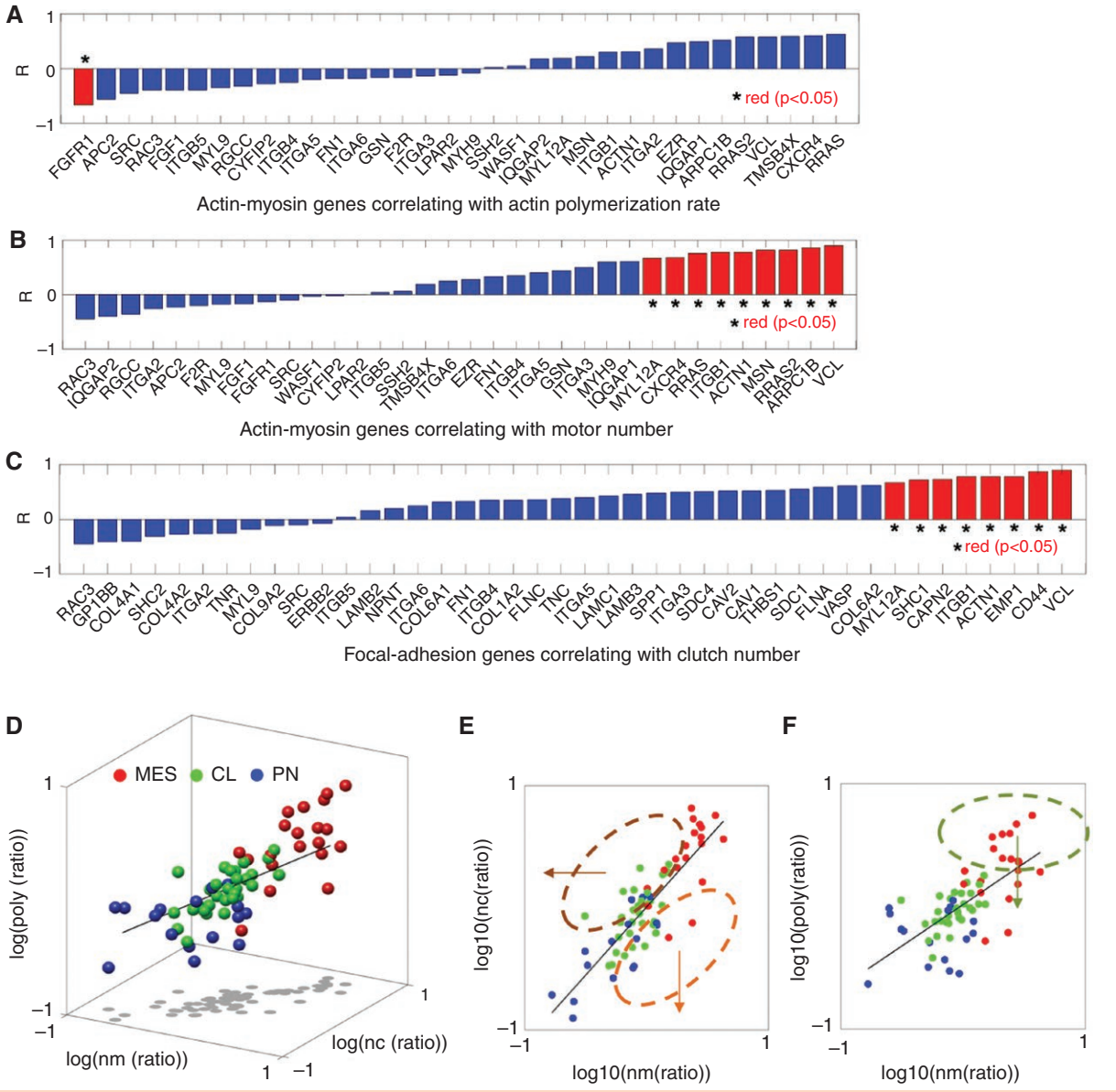

Figure 5. CMS-based transcriptomic biomarkers lead to targeting strategies for glioblastoma cell migration. We applied the pathway enrichment analysis to the 1177 differential genes between Mayo MES and PN cell lines (method: mRNA expression analysis) using the KEGG database[34] with the false discovery rate (FDR)-adjusted $P < .05$, and derived 29 enriched pathways (Supplementary Figure 7. We derived the actin-motor gene list (34 genes) based on the "Regulation of actin cytoskeleton" pathway, and the clutch gene list (42 genes) based on the "Focal adhesion" and "ECM-receptor interaction" pathways. Correlation analysis was applied to the mRNA expression ratios of the actin-motor (A, B) and clutch (C) genes in the 10 Mayo lines used in the present study (no mRNA data was available for the Mayo line 16) and their CMS parameter values, v_{poly} (A), n_m (B), n_c (C), respectively, along with their correlation coefficients (R) were sorted and plotted in (A–C) (significant correlation is marked with *). Highly correlated genes in (A) represent actin genes (RRAS, CXCR4, TMSB4X, RRAS2, ARPC1B). Significantly correlated genes in (B) represent motor genes (MSN, ACTN1, MLY12A; MYH9 was added). Significantly correlated genes in (C) represent clutch genes (VCL, CD44, EMP1, ITGB1, CAPN2, SHC1). Physical parameter ratios (n_m, n_c, v_{poly}) were estimated by averaging the mRNA expression ratios of these actin, motor, and clutch genes for each Mayo PDX line (66 lines) and plotted in the 3D CMS parameter space (D) with 2D projections (E, F). Actin polymerization rate is slightly linearly correlated with motor-clutch number in (D) (actin = motor*0.3 ($P = .01$) + clutch*0.3 ($P = .07$) + 0.01). The clutch number is significantly correlated with the motor number in (E) (clutch = motor ($P < .001$) + 0.01). Actin polymerization rate is significantly correlated with motor number in (F) (actin = motor*0.7 ($P < .001$) + 0.01).

and were chosen to represent actin genes. MSN, ACTN1, MLY12A; MYH9 were significantly correlated with a motor number (Figure 5B) and represent motor genes (MYH9 was added as a key component in myosin assembly with $P = .067$ slightly above our cutoff of $P = .05$). VCL, CD44, EMP1, ITGB1, CAPN2, and SHC1 were significantly correlated with a clutch number (Figure 5C) and represent clutch genes. By averaging the mRNA ratios of these correlated

genes (5 actin genes, 4 motor genes, and 6 clutch genes), we estimated the physical parameter ratios for each Mayo PDX line, plotted in the 3D CMS parameter space of (n_m, n_c, v_{poly}) (Figure 5D) with 2D projections (Figure 5E and F). MES lines (red dots in Figure 5) had higher (n_m, n_c, v_{poly}) compared with PN lines (blue dots in Figure 5), with CL lines having intermediate values (green dots in Figure 5). The trends of the highly balanced motor and clutch number with correlated F-actin polymerization (Figure 5D–F) do not change when a smaller focused subset of 3 genes was chosen for each parameter (Supplementary Figure 8). Even a single gene can largely reflect this same trend (Supplementary Figure 9).

We also acquired RNAseq normalized TPM values from TCGA (151 patients, 20 531 genes) and applied Cox regression analysis on migration gene expression and patient survival for both Mayo and TCGA patients, and we found 17 genes were significantly correlated with patient survival, and TCGA patients have more correlated genes than Mayo patients (Supplementary Figure 10). Within these genes, MYL12A and ITGB1 can be regarded as representative motor and clutch genes, which is the possible mechanism driving the correlation with patient survival. There are fewer correlated genes in MES (Supplementary Figure 11) and PN (Supplementary Figure 12) patients, with larger patient variation, due to the limited number of patients. In the end, our approach is an integration of mechanistic modeling and data science approaches.

Discussion

In this study, we used the physics-based motor-clutch model, termed here the CMS[26] (Figure 1A), to mechanistically parameterize and predict glioblastoma cell migration mechanics and speed. We reduced the 11-dimensional parameter space of the CMS (see Table 1) into 3 dimensions based on their parameter sensitivities (Figure 1B) and identified 3 fundamental physical parameters: motor number, clutch number, and actin polymerization rate that can uniquely govern cell migration (Figure 1C and D). We found significant heterogeneity in glioblastoma patient cell migration across subtypes and sources (Figure 2) and derived the physical parameter values for each cell line by fitting their cell migration with the CMS predictions (Figure 3). Despite their heterogeneity, glioblastoma cells had balanced motor/clutch ratios ($n_c/n_m \sim 0.75$) to produce robust cell migration and traction force (Figures 1C and 3A). In addition, we found consistent trends by molecular subtype, with Mayo MES cells having higher motor-clutch number and F-actin polymerization rate relative to Mayo PN cells (Figure 3), resulting in higher motility and F-actin flow (Figure 2E). Similarly, UCSD MES cells had a higher F-actin polymerization rate relative to the UCSD PN cells (Figure 3) resulting in faster migration (Figure 2E). Moreover, the CMS accurately predicted the differential sensitivities between MES and PN cells to cytoskeletal drug perturbations (Figure 4). Finally, we derived a list of motor-clutch-associated genes in the Mayo cells having mRNA expression correlating with the physical parameters of Mayo cells, which can be used to predict CMS cell migration parameters and speeds. Overall, we describe a simplified 3D physics-based framework for mechanically parameterizing individual glioblastoma patients and connecting biomechanics to clinical transcriptomic data, which can potentially be used to predict cell migration and drug responses in glioblastoma cells.

Our present study used 2D measurements with a range of stiffnesses that have been reported for brain tissue (1–10 kPa).[36] In addition, our recent studies find that 2D measurements are predictive of 1D confined migration in vitro[37] and of migration in 3D brain tissue ex vivo.[5,8] Our previous studies showed that the motor-clutch model is relevant to glioblastoma cell migration in brain tissue.[5,7,831] We also note that the 2D in vitro migration speeds are predictive of clinical MRI features.[31]Therefore, we have evidence that the 2D biomechanical measurements we are making here will be directly relevant to 3D migration in brain. We found that glioblastoma MES cells have faster migration than PN and CL cells on 2D compliant PA gels, which is consistent with the 3D invasion of glioblastoma spheroids in Munthe et al..[38] Piao et al.[39] similarly found the glioblastoma cell lines similar to the MES subtype had higher invasive capacity and motility compared with other subtypes. To provide the biophysical mechanisms of the differential cell motility, we parameterized the cell migration of glioblastoma cells with the CMS and found the higher F-actin polymerization rate best explained the faster migration of the MES cells relative to the PN cells (Figures 3 and Supplementary Figure 4). In the CMS simulation, a higher F-actin polymerization rate promotes cell protrusion dynamics, with longer protrusion length and highly fluctuating traction force, causing highly unbalanced protrusion forces, highly polarized cell morphology, and hence faster migration (Figure 1C and D). Adebowale et al.[28] applied the CMS simulation coupled with viscoelastic substrate and also confirmed that the significant filopodia dynamics with longer filopodia length and lifetime resulted in faster cell migration of fibrosarcoma cells on fast-relaxing viscoelastic gels, demonstrating the protrusion dynamics promoting cell motility in vitro. Therefore, F-actin polymerization becomes a potential target to alter glioblastoma cell motility, and the CMS can potentially predict the patient-specific cell motility and treatment responses.

The subtype definitions/classifiers have shifted over time since the original classification by Phillips et al.[14] (PN, Proliferative, and MES) and we are using the published classifications for these PDX collections, following Wang et al.[16] (PN, CL, and MES), which was itself an update from earlier work by Verhaak et al.[15] (PN, Neural, CL, and MES). Wang et al.[16] concluded that the Neural subtype was likely due to contamination from adjacent brain tissue. The recent single-cell RNAseq work (Neftel et al.[40]) has supported the view of 4 subtypes, rather than 3, along with both intratumoral heterogeneity and plasticity. Even so, Neftel et al.[40] described how their classification can be mapped onto the previous Wang-Verhaak classification,[16] with oligodendrocyte-progenitor/neural-progenitor (OPC/NPC) being associated with PN, astrocyte being associated with the CL subtype, and the same MES subtype. Overall, for the past 15 years, the field has had a PN (OPC/NPC) to MES axis, with the CL (AC) subtype being a robust intermediate substate. Hence the PN/CL/MES classification

used in our study is very much in line with the current standard in the field, and the subtypes for the Mayo PDX and UCSD PD lines have been published.[32,33] In the present study, we account for the variability on a patient-by-patient basis. Heterogeneity and plasticity are clearly potential confounders of simple categorizations. However, if these were strong effects, then the subtype classification of patients based on a single tissue sample would not yield consistent patterns with mechanistic measurements such as ours, that is, a similar pattern of the model-based parameterization of n_m, n_c, v_{poly} throughout patient cell lines. In particular, we found that MES cells had higher estimated v_{poly}, which enables faster migration, and higher motor-clutch levels (Figures 3B and 5D). Our results suggest that v_{poly} and motor-clutch ratio, and their associated genes, may be better predictors of functional subtype than the traditional PN/CL/MES classification. However, we believe that this will require prospective tests in more in vivo–like settings in the future.

By correlating with the CMS parameters, we found the representative actin, motor, and clutch genes in Figure 5A–C. Based on the predicted cell migration in Figure 1C, we can identify patient-specific strategies to target the cell migration of glioblastoma. For example, for the patients with higher motor-clutch ratios (Figure 5E, orange dotted line), we can inhibit adhesion clutches resulting in free-flowing conditions (Figure 1C and D, Condition II). For patients with lower motor-clutch ratios (Figure 5E, brown dotted line), we inhibit myosin motors resulting in stalled conditions (Figure 1C and D, Condition III). For patients with a higher actin polymerization rate (Figure 5F, green dotted line, mostly MES lines), we then inhibit the actin polymerization to block the migration. We also applied the Cox regression analysis on the migration gene expression and patient survival in the Mayo and TCGA cohorts. Among the genes highly correlated with patient survival (Supplementary Figure 10), ITGB1, ITGA5, ITGA3 showed significant association with the patient survival in Malric et al.,[41] consistent with our results. The negative correlation between CD44 levels and PN patient survival aligned with Klank et al.'s.[7] Collagen (COL9A2, COL6A2, COL4A1, COL4A2) enrichment is associated with poor prognosis of glioblastoma patients.[42–44] Overall, these genes are significantly hazardous to patient survival, and some of them (ITGB1, CD44) are also closely associated with the CMS parameters, which makes them potential markers and targets to enhance patient survival based on patient-specific transcriptomic information.

Our study has some limitations and points to future work. While we would expect that the faster migration speed in MES cells may contribute to the lower survival found in MES patients vs. CL or PN,[15,16] we suspect that other confounding variables need to be included in the further analysis, such as age[2] and immune response[15,16] in order to better predict patient survival. While we had hoped to identify genes that are associated with the F-actin polymerization rate, we found only 1 statistically significant correlation. It is likely that we will need a larger cohort of patient cells with greater sequencing depth in actin, motor, and clutch genes. In order to be of clinical utility, future work will need to prospectively test transcriptomic predictions in terms of cell migration and drug sensitivities, rather than the retrospective relationships identified in the present study. Even so, the overall results provide a proof of concept that CMS-based mechanical biomarkers can be used to describe cell migration dynamics, predict differential drug sensitivities, and identify correlations with mechanistically relevant mRNA transcript levels. This platform allows us to predict on a patient-by-patient basis the most effective intervention (ie intervention with the greatest predicted sensitivity) to suppress cancer cell migration, similar to how migration speed can be estimated via machine learning–based detection of features in clinical MRI images.[31]

Supplementary material

Supplementary material is available online at *Neuro-Oncology Advances* (https://academic.oup.com/noa).

Keywords:

cell migration | biophysical modeling | glioblastoma subtypes | motor-clutch model | patient-derived cell lines

Funding

This work was supported by the National Institutes of Health (grant numbers U54CA210190, P01CA254849 to D.J.O.).

Conflict of interest statement

None declared.

Authorship statement

Conceptualization: J.H., M.M., D.J.O. Funding acquisition: D.J.O. Cell line development: J.N.S., C.C.C. Investigation, methodology, data analysis, visualization: J.H., M.M. Simulation and modeling: J.H. mRNA expression analysis: J.H., T.J. Supervision: D.J.O. Writing (original draft): J.H., M.M., D.J.O. Writing (review and editing): all authors.

Affiliations

Department of Neurosurgery, Rhode Island Hospital—Brown University Health, Providence, Rhode Island, USA (J.H.); Department of Biomedical Engineering, University of Minnesota—Twin Cities, Minneapolis, Minnesota, USA (M.M., D.J.O.); Department of Pediatrics, University of Minnesota—Twin Cities, Minneapolis, Minnesota, USA (T.J.); Department of Radiation Oncology, Mayo Clinic Rochester, Rochester,

Minnesota, USA (J.N.S.); Department of Neurosurgery, Brown University, Providence, Rhode Island, USA (C.C.C.)

References

1. Stupp R, Hegi ME, Mason WP, et al.; European Organisation for Research and Treatment of Cancer Brain Tumour and Radiation Oncology Groups; National Cancer Institute of Canada Clinical Trials Group. Effects of radiotherapy with concomitant and adjuvant temozolomide versus radiotherapy alone on survival in glioblastoma in a randomised phase III study: 5-year analysis of the EORTC-NCIC trial. *Lancet Oncol.* 2009;10(5):459–466.
2. Ostrom QT, Gittleman H, Liao P, et al. CBTRUS statistical report: primary brain and central nervous system tumors diagnosed in the United States in 2007–2011. *Neuro-Oncol.* 2014;16(suppl 4):iv1–i63.
3. Davis ME. Glioblastoma: overview of disease and treatment. *Clin J Oncol Nurs.* 2016;20(5 Suppl):S2–S8.
4. De Vleeschouwer S, ed. *Glioblastoma*. Brisbane: Codon Publications; 2017.
5. Liu CJ, Shamsan GA, Akkin T, Odde DJ. Glioma cell migration dynamics in brain tissue assessed by multimodal optical imaging. *Biophys J.* 2019;117(7):1179–1188.
6. Stupp R, Hegi ME, Gorlia T, et al.; European Organisation for Research and Treatment of Cancer (EORTC); Canadian Brain Tumor Consortium; CENTRIC Study Team. Cilengitide combined with standard treatment for patients with newly diagnosed glioblastoma with methylated MGMT Promoter (CENTRIC EORTC 26071-22072 Study): a multicentre, randomised, open-label, phase 3 trial. *Lancet Oncol.* 2014;15(10):1100–1108.
7. Klank RL, Decker Grunke SA, Bangasser BL, et al. Biphasic dependence of glioma survival and cell migration on CD44 Expression Level. *Cell Rep.* 2017;19(3):668.
8. Anderson SM, Kelly M, Odde DJ. Glioblastoma cells use an integrin- and CD44-mediated motor-clutch mode of migration in brain tissue. *Cell Mol Bioeng.* 2024;17(2):121–135.
9. Girda E, Hou J, Nelson D, et al. Phase I trial of daily subcutaneous SPL-108 injections in combination with paclitaxel in patients with platinum resistant CD44+ advanced ovarian epithelial cancer. *Int J Gynecol Cancer.* 2022;32(8):1032–1038.
10. Ivkovic S, Beadle C, Noticewala S, et al. Direct inhibition of myosin II effectively blocks glioma invasion in the presence of multiple motogens. *Mol Biol Cell.* 2012;23(4):533–542.
11. Picariello HS, Kenchappa RS, Rai V, et al. Myosin IIA suppresses glioblastoma development in a mechanically sensitive manner. *Proc Natl Acad Sci USA.* 2019;116(31):15550–15559.
12. Radnai L, Surman M, Hafenbreidel M, et al. Discovery of selective inhibitors for in vitro and in vivo interrogation of skeletal Myosin II. *ACS Chem Biol.* 2021;16(11):2164–2173.
13. Hayashi K, Michiue H, Yamada H, et al. Fluvoxamine, an anti-depressant, inhibits human glioblastoma invasion by disrupting actin polymerization. *Sci Rep.* 2016;6:23372.
14. Phillips HS, Kharbanda S, Chen R, et al. Molecular subclasses of high-grade glioma predict prognosis, delineate a pattern of disease progression, and resemble stages in neurogenesis. *Cancer Cell* 2006;9(3):157–173.
15. Verhaak RGW, Hoadley KA, Purdom E, et al.; Cancer Genome Atlas Research Network. Integrated genomic analysis identifies clinically relevant subtypes of glioblastoma characterized by abnormalities in PDGFRA, IDH1, EGFR, and NF1. *Cancer Cell* 2010;17(1):98–110.
16. Wang Q, Hu B, Hu X, et al. Tumor evolution of glioma-intrinsic gene expression subtypes associates with immunological changes in the microenvironment. *Cancer Cell* 2017;32(1):42–56.e6.
17. Rahman M, Reyner K, Deleyrolle L, et al. Neurosphere and adherent culture conditions are equivalent for malignant glioma stem cell lines. *Anat Cell Biol* 2015;48(1):25–35.
18. Mitchison T, Kirschner M. Cytoskeletal dynamics and nerve growth. *Neuron.* 1988;1(9):761–772.
19. Lauffenburger DA, Horwitz AF. Cell migration: a physically integrated molecular process. *Cell.* 1996;84(3):359–369.
20. Hu K, Ji L, Applegate KT, Danuser G, Waterman-Storer CM. Differential transmission of actin motion within focal adhesions. *Science.* 2007;315(5808):111–115.
21. Chan CE, Odde DJ. Traction dynamics of filopodia on compliant substrates. *Science.* 2008;322(5908):1687–1691.
22. Elosegui-Artola A, Bazellières E, Allen MD, et al. Rigidity sensing and adaptation through regulation of integrin types. *Nat Mater.* 2014;13(6):631–637.
23. Estabridis HM, Jana A, Nain A, Odde DJ. Cell migration in 1D and 2D nanofiber microenvironments. *Ann Biomed Eng.* 2018;46(3):392–403.
24. Vicente-Manzanares M, Ma X, Adelstein RS, Horwitz AR. Non-muscle myosin II takes centre stage in cell adhesion and migration. *Nat Rev Mol Cell Biol.* 2009;10(11):778–790.
25. Gardel ML, Schneider IC, Aratyn-Schaus Y, Waterman CM. Mechanical integration of actin and adhesion dynamics in cell migration. *Annu Rev Cell Dev Biol.* 2010;26:315–333.
26. Bangasser BL, Shamsan GA, Chan CE, et al. Shifting the optimal stiffness for cell migration. *Nat Commun.* 2017;8:15313.
27. Hou JC, Shamsan GA, Anderson SM, et al. Modeling distributed forces within cell adhesions of varying size on continuous substrates. *Cytoskeleton (Hoboken, N.J.)* 2019;76(11–12):571–585.
28. Adebowale K, Gong Z, Hou JC, et al. Enhanced substrate stress relaxation promotes filopodia-mediated cell migration. *Nat Mater.* 2021;20(9):1290–1299.
29. Isomursu A, Park K-Y, Hou J, et al. Directed cell migration towards softer environments. *Nat Mater.* 2022;21(9):1081–1090.
30. Lee SH, Hou JC, Hamidzadeh A, et al. A molecular clock controls periodically driven cell migration in confined spaces. *Cell Syst* 2022;13(7):514–529.e10.
31. Mulford K, McMahon M, Gardeck AM, et al. Predicting glioblastoma cellular motility from in vivo MRI with a radiomics based regression model. *Cancers* 2022;14(3):578.
32. Vaubel RA, Tian S, Remonde D, et al. Genomic and phenotypic characterization of a broad panel of patient-derived xenografts reflects the diversity of glioblastoma. *Clin Cancer Res.* 2020;26(5):1094–1104.
33. Akers JC, Ramakrishnan V, Kim R, et al. miRNA contents of cerebrospinal fluid extracellular vesicles in glioblastoma patients. *J Neurooncol.* 2015;123(2):205–216.
34. Ogata H, Goto S, Sato K, et al. KEGG: Kyoto encyclopedia of genes and genomes. *Nucleic Acids Res.* 1999;27(1):29–34.
35. Bangasser BL, Rosenfeld SS, Odde DJ. Determinants of maximal force transmission in a motor-clutch model of cell traction in a compliant microenvironment. *Biophys J.* 2013;105(3):581–592.
36. Hormuth DA, Weis JA, Barnes SL, et al. A mechanically coupled reaction-diffusion model that incorporates intra-tumoural heterogeneity to predict in vivo glioma growth. *J R Soc Interface.* 2017;14(128):20161010.
37. Prahl LS, Stanslaski MR, Vargas P, Piel M, Odde DJ. Predicting confined 1D cell migration from parameters calibrated to a 2D motor-clutch model. *Biophys J.* 2020;118(7):1709–1720.
38. Munthe S, Sørensen MD, Thomassen M, et al. Migrating glioma cells express stem cell markers and give rise to new tumors upon xenografting. *J Neurooncol.* 2016;130(1):53–62.

39. Piao Y, Liang J, Holmes L, et al. Acquired resistance to Anti-VEGF therapy in glioblastoma is associated with a mesenchymal transition. *Clin Cancer Res*. 2013;19(16):4392–4403.
40. Neftel C, Laffy J, Filbin MG, et al. An integrative model of cellular states, plasticity, and genetics for glioblastoma. *Cell*. 2019;178(4):835–849.e21.
41. Malric L, Monferran S, Gilhodes J, et al. Interest of integrins targeting in glioblastoma according to tumor heterogeneity and cancer stem cell paradigm: an update. *Oncotarget* 2017;8(49):86947–86968.
42. Comba A, Faisal SM, Dunn PJ, et al. Spatiotemporal analysis of glioma heterogeneity reveals COL1A1 as an actionable target to disrupt tumor progression. *Nat Commun*. 2022;13(1):3606.
43. Zhu J, Lin Q, Zheng H, Rao Y, Ji T. The pro-invasive factor COL6A2 serves as a novel prognostic marker of glioma. *Front Oncol*. 2022;12:897042.
44. Shin H-J, Gil M, Lee I-S. Association of elevated expression levels of COL4A1 in stromal cells with an immunosuppressive tumor microenvironment in low-grade glioma, pancreatic adenocarcinoma, skin cutaneous melanoma, and stomach adenocarcinoma. *J Pers Med* 2022;12(4):534.